Fast spike pattern detection using the correlation integral

M. Christen,[1] A. Kern,[1] A. Nikitchenko,[1,2] W.-H. Steeb,[3] and R. Stoop[1,*]

[1]*Institute of Neuroinformatics, University / ETH Zürich, Winterthurerstrasse 190, 8057 Zürich, Switzerland*
[2]*Saint-Petersburg State Polytechnical University, Polytechnicheskaya str. 29, 195251 Saint-Petersburg, Russia*
[3]*Department of Applied Mathematics and Nonlinear Studies, Rand Afrikaans University, P.O. Box 524, Auckland Park 2006,
South Africa*

Conventional approaches to detect patterns in neuronal firing are template based. As the pattern length increases, the number of trial patterns to be tested leads to strongly divergent computational costs. To remedy this problem, we propose a different statistical approach, based on the correlation integral. Applications of our method to model and neuronal data demonstrate its reliability, even in the presence of noise. Additionally, our investigation provides interesting insights into the nature of correlation-integral anomalies.

I. INTRODUCTION

Biological neural systems can be viewed as an alternative information processing paradigm, that often proves far more efficient than conventional signal processing. Although the underlying structures (neurons and their connectivity) can be accurately modeled by electronic circuits [1], the principles according to which they process information are not well understood. Growing evidence, however, suggests that neuronal circuits work according to distributed parallel processing principles, and that neuronal information encoding differs from that of traditional signal processing [2].

In neural information processing systems, activity is manifested as spikes. Temporal recordings of firing events provide interspike interval (ISI) series. It is expected that aspects of the processed information are encoded in the form of structures contained in the ISI series. Patterns, however, are not the only method of neural information encoding. Whereas some neurons indeed specialize in firing in terms of patterns (due to their morphology, or their embedding in the network [3]), others prefer firing randomly (which has led to the Poissonian firing assumption [4]). For a given neuron, its firing characteristics appears to be stable in time. Recently, a computational model has been proposed wherein this coexistence proves advantageous [5].

Consequently, the detection of pattern occurrences can be considered a fundamental step in the analysis of the neural computation. Patterns are defined as those parts of the ISI series that repeat significantly more often than they would in a randomized series based upon the identical distribution [6]. The standard approach to the identification of patterns is to systematically predefine pattern templates and to count their frequency of occurrence (*template-based methods* [7,8]). Defining the length of a pattern as the number of the ISI's involved, only patterns of lengths from 1 to 5 have been reported [9,10]. Template-based methods suffer from two fundamental difficulties. First, the detection relies on the set of pre-chosen templates. As the patterns are *a priori* unknown, large template sets are required to include all potential patterns to be tested against. Second, due to the omnipresent noise, patterns cannot be expected to repeat perfectly, which implies having to choose a tolerance for template matching. Adopted tolerances range from fractions of one [11] to a few milliseconds [8], demonstrating the difficulty in determining the required accuracy. As an illustration, let $\{x_1, x_2, \ldots, x_L\}$, where $x_i > 0$, be an ISI series with $x_{\min}$ denoting the smallest and $x_{\max}$ the largest element. Templates have the form $(t_1 \pm \tilde{t}, t_2 \pm \tilde{t}, \ldots, t_k \pm \tilde{t})$, with template length k and tolerance $\tilde{t}$. The number of operations required for unbiased testing can then be estimated as follows. An optimal grid width of $\Delta t = 2\tilde{t}$ yields $N = \lceil x_{\max} - x_{\min}/\Delta t \rceil$ values to test, and N^k templates to match. Moreover, an unbiased template analysis requires choosing a set T of distinct tolerances. This leads to $\sim kT(L-k+1)N^k$ numbers that need to be compared.

It is evident that an efficient template analysis can only be performed for small k, which may explain the short pattern lengths reported in the literature. For an extended investigation, tools that detect the presence of patterns, find elements t_i composing the templates and estimate k are desired. Histograms and correlation functions fall short as reliable indicators. We propose to use the correlation integral as a purely statistical, bias-free tool to detect the presence of patterns. This approach is computationally inexpensive (number of pairs of numbers to compare $\sim kN^2$) and significantly reduces the set of potential templates to be tested. The underlying algorithm is well known and optimized implementations are widely used. In addition, our contribution sheds new light on widely observed anomalies of the correlation integral that are generally not well understood.

II. CORRELATION INTEGRAL METHOD

The correlation integral was originally designed for the determination of the correlation dimension [12,13]. The purpose of our paper is to explore its potential for the detection of patterns in neuronal spike trains. First, we briefly introduce the correlation integral, and elucidate its ability to detect clusters. Second, we address its application to ISI pat-

_____

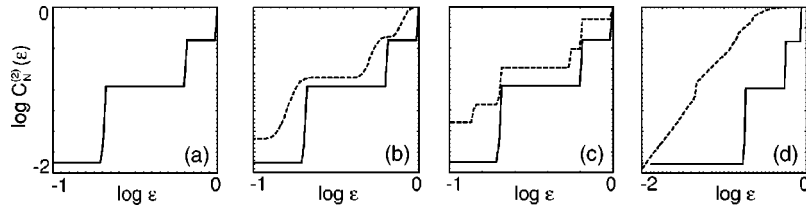*Corresponding author. FAX: +41-1-635-3053. Electronic address: ruedi@ini.phys.ethz.ch

FIG. 1. Log-log plot steps from different ISI models ($m=2$; Euclidean norm; $\log \equiv \log_2$). (a) low-noise case (noise $\pm 1\%$; solid line in all four plots), (b) noise $\pm 10\%$, (c) unstable periodic orbits, (d) patterns within noisy background.

terns. Third, we evaluate to what extent the method is helpful when determining ISI pattern lengths.

Consider an arbitrary scalar time series of measurements $\{x_i\}$, $i=1,\ldots,L$, where L denotes the length of the time series. From these data, embedded points $\xi_k^{(m)}$ are constructed: $\xi_k^{(m)}=\{x_k, x_{k+1}, \ldots, x_{k+(m-1)}\}$, where m is called the embedding dimension. This *coordinate-delay construction* is standard in nonlinear dynamics. Its purpose is to reconstruct the complete underlying (in general: high-dimensional) dynamics from partial, generally scalar, measurements [14–19]. From the embedded data, the *correlation integral* is calculated as

$$C_N^{(m)}(\epsilon) = \frac{1}{N(N-1)}\sum_{i \neq j} \theta(\epsilon - \|\xi_i^{(m)} - \xi_j^{(m)}\|),$$

where $\theta(x)$ is the Heaviside function [$\theta(x)=0$ for $x \leq 0$ and $\theta(x)=1$ for $x>0$] and N is the number of embedded points ($N \leq L-m+1$). Different norms can be used to compute $C_N^{(m)}(\epsilon)$. In most cases, the maximum norm is advantageous, as this choice speeds up the computation, and allows an easy comparison of results obtained for different embedding dimensions. Degeneracies introduced by this choice are removed by adding a small amount of noise. Alternatively, the Euclidean norm is often used.

The connection between $C_N^{(m)}(\epsilon)$ and patterns is surprisingly simple: For the calculation of $C_N^{(m)}(\epsilon)$, an embedded point $\xi_0^{(m)}$ is chosen at random. Then, the number of points entering its ϵ neighborhood is evaluated, as ϵ is enlarged. If the point belongs to a cluster, many points will join the ϵ neighborhood. Once the cluster size is reached, fewer points are recruited, leading to a slower increase of $C_N^{(m)}(\epsilon)$. When, as required by the correlation integral, an average over different points is taken, pieces of fast increase of $C_N^{(m)}(\epsilon)$ interchange with pieces of slow increase. This leads to a staircaselike graph of the correlation integral. The denser the clustered regions, the more prominent the stepwise structures. Plotting $C_N^{(m)}(\epsilon)$ on a log-log scale not only preserves these structures but enhances the representation of small-scale steps.

To show the emergence of steps, we constructed a series from a repetition of the sequence $\{1,2,4\}$, where the sequence numbers can be interpreted as ISI durations measured in ms. The embedding of this series for $m=2$ leads to three clusters, represented by the points $P_1=\{1,2\}$, $P_2=\{2,4\}$, and $P_3=\{4,1\}$. Calculating the correlation integral and plotting $\log C_N^{(m)}(\epsilon)$ against $\log \epsilon$ does indeed lead to a clean-cut staircase structure [Fig. 1(a)]. Throughout the paper we use loga-

rithms to the base 2 for our numerical results.

In practical applications of the method, the steps in the log-log plot generally become less salient due to influences that will be discussed below. In this case, the difference quotient $\Delta \log C_N^{(m)}(\epsilon_i) := \log C_N^{(m)}(\epsilon_{i+1}) - \log C_N^{(m)}(\epsilon_i)$, which approximates the derivative of the correlation integral, is a more sensitive indicator of clusters. For small ϵ neighborhoods, the log-log plot is affected by strong statistical fluctuations. These regions, however, are easily identified and excluded from the analysis.

III. SMEARED LOG-LOG STEPS

In natural systems, the steps are smeared. We investigated three causes. The first is noise, which is naturally present in measured ISI series. This can be modeled by adding uniform noise to our ISI series $\{1,2,4,1,2,4\ldots\}$. Added noise causes the point clusters in the embedding space to become more dispersed. Consequently the effects of small amounts of noise will only be visible at the step boundaries. As the noise increases, its effects penetrate towards the centers. This is visible in Fig. 1(b) where the horizontal parts of the steps have become narrower, and the vertical parts less steep.

Second, the generator of the ISI series could be chaotic in nature. In this case, a distance from a given unstable periodic orbit grows at $e^{t\lambda}$, where t denotes the time and λ is the (positive) Lyapunov exponent of the orbit. This implies that the repetition of any sequence is less likely the larger λ. Moreover, because the decay from the unstable orbit is deterministic, additional (pseudo) orbits will emerge, increasing the number of steps. Recently, a simple chaos control method has been found, that has the potential of being implemented in biological neural networks [20,21]. We can simulate this situation with a simple series composed as follows: With probability $p_1=0.5$ we take the whole sequence $\{1,2,4\}$, with $p_2=0.31$ the subsequence $\{1,2\}$, and with $p_3=0.19$ the subsequence $\{1\}$ (this choice leads to $p_1/p_2 \simeq p_2/p_3$). The results [Fig. 1(c)] show five instead of three steps, indicating that additional orbits have been generated.

A third option is that patterns occur within a noisy background. In this case, the pattern only appears intermittently. As a consequence, the fraction of points belonging to clusters in the embedding space is diminished, implying that the steps in the log-log plot become less prominent. To simulate this situation, we took with probability $p=0.5$ the sequence $\{1,2,4\}$, otherwise three interspike intervals were randomly drawn from the interval $(0,4]$. The results [Fig. 1(d)] show that the number of steps indeed remains unaffected, but the
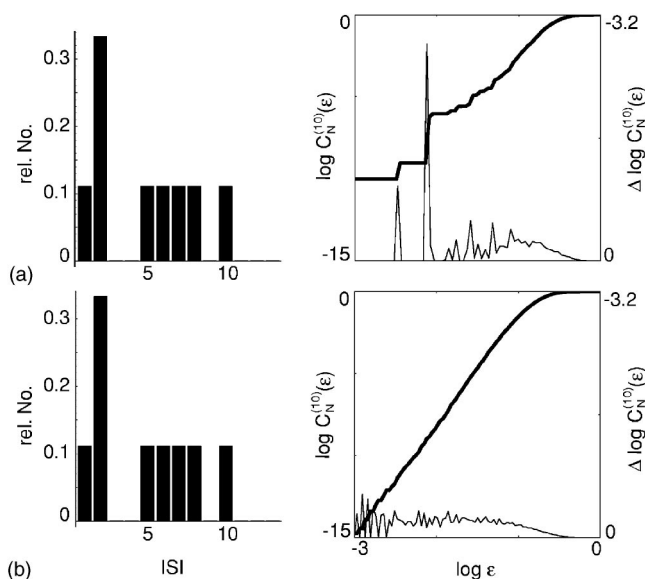
FIG. 2. Series composed of patterns (a) and series constructed by a random selection of intervals (b), with identical ISI distributions (left). Steps [y-axis: $\log C^{(10)}(\epsilon)$, thick line] only emerge in the presence of patterns. Steps are reflected by peaks in the difference quotient plot [y-axis: $\Delta \log C^{(10)}(\epsilon)$, thin line], respectively ($m=10$; Euclidean norm; $\log \equiv \log_2$).

steps themselves have become much less pronounced.

In natural systems, more than one pattern may be present. To analyze this situation, we assembled a series by randomly choosing among sequences {2,6,10}, {8,2,1}, {2,7,5}. To contrast this with random firing, we assembled a second series by randomly selecting intervals from the concatenated set {2,6,10,8,2,1,2,7,5}. Thus both series are based on identical probability distributions. Our analysis [Figs. 2(a) and

TABLE I. Maximum number of steps $s(m,n)$ as a function of the embedding dimension m and pattern size n.

Pattern size n	Embedding dimension m						
	1	2	3	4	5	6	7
1	0	0	0	0	0	0	0
2	1	1	1	1	1	1	1
3	3	2	1	1	1	1	1
4	6	4	3	2	2	2	2
5	10	8	6	4	2	2	2
6	15	12	9	7	5	3	3

2(b), respectively] shows that steps (peaks in the quotient plot) emerge only if patterns are present. Thus we conclude that our method is able to reliably indicate the presence of patterns.

IV. PATTERN LENGTH ESTIMATION

Once the presence of patterns has been established, an estimate of the pattern length can be given. That this is possible is motivated by the following argument. Using the maximum norm, the distance between two points is defined as the largest coordinate difference. An increase of the embedding dimension yields ever more coordinate pairs, causing the presence of a particularly large difference to dominate. Consequently, the number of steps calculated for pattern length n decreases with increased embedding dimension m.

The maximum number of steps $s(m,n)$ can be numerically computed as follows. We start from a series generated by a repetition of a sequence of length n. Additionally, we
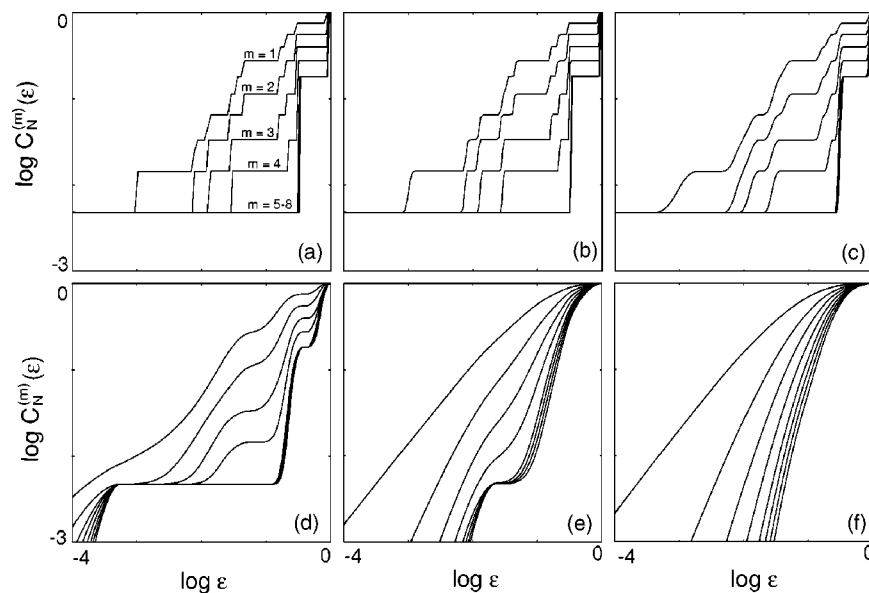

FIG. 3. (a) The number of steps decreases as the embedding dimension increases ($m=1,\ldots,8$; sequence length: 5; $\log \equiv \log_2$). At $m=1$ there are ten steps, in agreement with Table I. (b)–(f): Behavior in the presence of additive noise (noise levels 8%, 32%, 128%, 512%, and 1024%, see text). The number of steps for $m=1,\ldots,4$ decreases for increased noise. The clearest step always emerges for $n=5$, indicating a sequence of length 5.
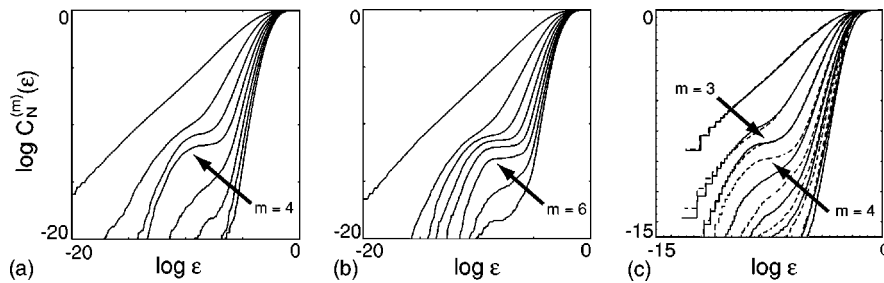
FIG. 4. Pattern-length indicator $m=n$: Sequences of length n in a homogeneous Poisson background (embedding dimensions $m=1,\ldots,8$; $\log \equiv \log_2$). (a) $n=4$: most pronounced step at $m=4$; (b) $n=6$: most pronounced step at $m=6$. (c) Sequences of $n=3$ and $n'=4$ included with different ratios (3:1 solid lines, 1:3 dashed lines): most pronounced step where m equals the length of the dominating sequence.

require that the elements $\{x_1,\ldots,x_n\}$ yield distinct coordinate differences $|x_i-x_j|$. After choosing an embedding dimension m, n distinct embedded points are generated. On this set of points, the maximum norm induces classes of equal interpoint distances. The number of these classes equals $s(m,n)$. The actual calculation of $s(m,n)$ can be done using a computer program (which, however, exhausts ordinary computer capabilities very quickly), or by an unexpectedly involved analytical calculation. The closed expression for $s(m,n)$ is beyond the scope of this paper.

The lowest numbers $s(m,n)$ are given in Table I. They clearly confirm the anticipated decrease of the number of steps as a function of m. For the series generated from the sequence $\{5, 24, 37, 44, 59\}$, our correlation integral approach is able to reproduce the predicted decrease of $s(n,m)$ [Fig. 3(a)]: In embedding dimension $m=1$, all ten possible nonzero differences are visible. As m increases towards 5,

the number of steps decreases in accordance with Table I, remaining constant for $m>5$.

The behavior reported in Table I only holds if the series are created by repeating a pattern based on distinct intercoordinate differences. In more general cases, the exact determination of the pattern length is hampered by a basic difficulty: If one single step emerges, this can either be due to one pattern consisting of two consecutive ISI's, or two "patterns" of one ISI each. A greater number of steps further complicates this problem. As a consequence, Table I can only serve as a rough guideline.

Fortunately, a helpful indicator for the pattern length exists. A pattern will emerge in the embedded ISI series in its most genuine form (it is neither cut into pieces, nor spoilt by foreign points), if the pattern length equals the chosen embedding dimension ($m=n$). In Fig. 3(a), the most pronounced steps appear at $m=5$, correctly indicating a pattern of length $n=5$.
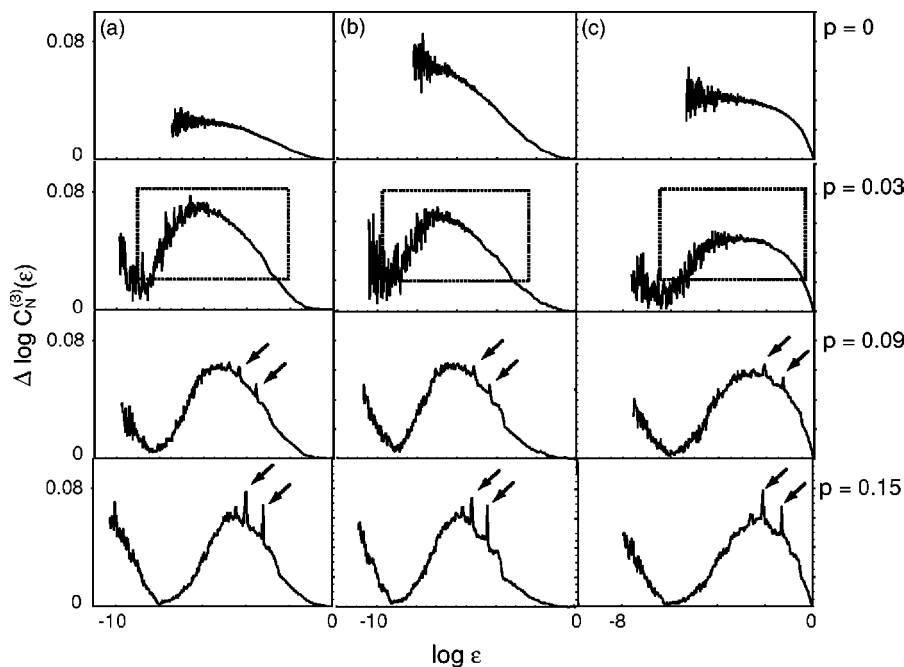

FIG. 5. Detection of sequences injected (with $p=0,0.03,0.09,0.15$) into random backgrounds based on the difference quotient: (a) Homogeneous Poisson background, (b) inhomogeneous Poisson background, (c) "white noise" background. Already at a low injection probability of $p=0.03$, a hump emerges (dashed boxes). At $p=0.09$, smaller peaks indicate the statistically significant accumulation of pattern-induced distances ($m=3$; $\log \equiv \log_2$).
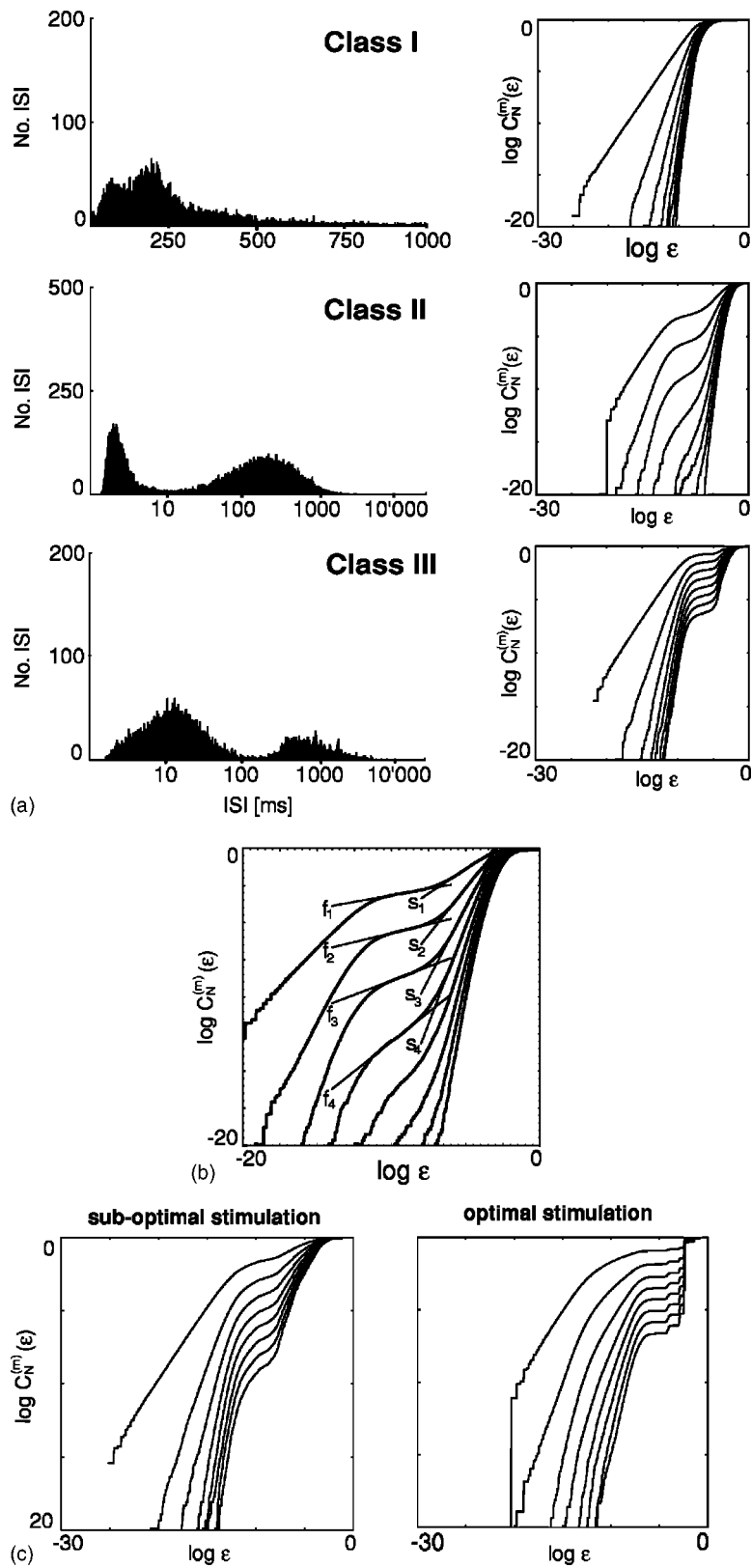
FIG. 6. Cat V1 ISI-data, in milliseconds. (a) Neurons based on bimodal ISI distributions (left panels) display distinct firing classes: Class I: noisy; class II: patterns in a random or incoherent background; class III: patterns ($m = 1, \ldots, 8$; $\log \equiv \log_2$). (b) Neuron of class II: The most pronounced steps appear at $m = 2$ and $m = 3$, indicating patterns of length 2 and 3. (c) Optimal stimulation of a class III neuron leads to a pattern sharpening effect.

TABLE II. Ratio of the flat slope (f_m) over the steep slope (s_m) of a step, as a function of the embedding dimension m, of the data shown in Fig. 6(b).

m	1	2	3	4
f_m/s_m	0.27	0.19	0.20	0.30

To investigate the reliability of the criterion in natural settings, noise was added to the series generated from the sequence {5, 24, 37, 44, 59}. For the following, we define the noise strength as the ratio of the noise sampling interval over shortest sequence interval. The results [Figs. 3(b)–3(f)] demonstrate that the pattern length can be reliably estimated up to a noise level of 512% [Fig. 3(e)], where the most pronounced step still appears at $m=5$. The number of steps for $m<5$ is affected by the noise: For $m=1$, for example, nine steps are present at 8% noise [Fig. 3(b)], seven steps at 32% [Fig. 3(c)], and three steps at 128% [Fig. 3(d)]. The step structure disappears if the noise level reaches the size of the largest sequence element [Fig. 3(f)]. Thus the observation that the most pronounced step appears at $m=n$, yields a valuable criterion for estimating the pattern length.

We found that this criterion also extends to less ideal settings. To illustrate, we injected the sequences {5, 25, 10, 2} and {5, 25, 10, 2, 17, 33}, each with probability $p=0.06$, into a noisy background generated by a homogeneous Poisson process with refractory period. The Poisson distribution was tuned to produce a mean identical with that of the patterns. The clearest steps emerge at the embedding dimensions 4 and 6 [Figs. 4(a) and 4(b)], showing that also in this case the pattern length can be estimated. We refined our investigation by varying the injection probabilities. Using the sequences {4, 17, 12} and {5, 25, 10, 2}, the first sequence was chosen with $p=0.12$ and the second with $p=0.04$. We compared this series with a series based on interchanged probabilities. The outcome is that the clearest steps emerge for $m=n$, where the pattern with the higher probability dominates [Fig. 4(c)]. If the two probabilities are similar, the estimation may be hampered by effects of interference. A means of quantifying the "clarity" of a step is to calculate the ratio between the slopes of the flat and of the steep part of the steps. Consistently, the embedding dimension for which the slope ratio reaches a minimum coincides with the pattern length.

Currently, alternative models of noisy backgrounds exist [4,22]. To show that our results hold regardless of which model applies, we injected the sequence {33, 14, 22} into backgrounds generated by (i) a homogeneous Poisson process with refractory period, (ii) an inhomogeneous, sinusoidally modulated Poisson process with refractory period, and (iii) a uniform random process on the interval (0, 46), using injection probabilities $p \in \{0, 0.03, 0.09, 0.15\}$. The results show that the nature of the noisy background has a negligible influence on the pattern detectability. Instead, the injection probability is decisive (Fig. 5). Whereas two sharp peaks are obtained for $p=0.15$ and $p=0.09$ (arrows), only one large hump emerges for $p=0.03$. A single broad peak indicates a reduced frequency of short intervals, which is the first indicator of patterns at lowest injection probability. Two narrow
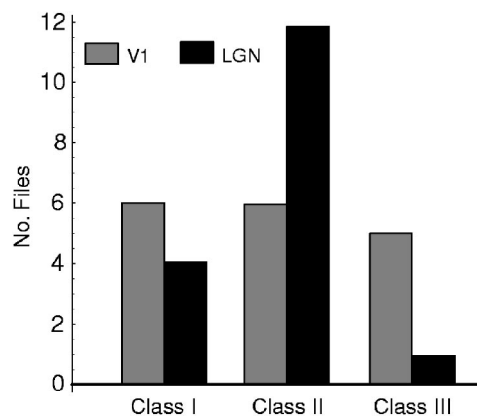

FIG. 7. Histogram of LGN and V1 data based on classes I–III.

peaks indicate the pattern-generated statistically significant accumulation of particular distances.

V. APPLICATION TO NEURONAL DATA

The method has been applied to extracellular field potential measurements of anesthetized cat neurons from striate cortex (V1) and lateral geniculate nucleus (LGN) (for details see Refs. [3] and [23]). Seventeen time series from four neurons of V1 and 17 time series from six neurons of LGN were analyzed.

Earlier investigations of V1 data [3,24] suggested the existence of three essentially stimulus-independent neuron classes: (I) the class of randomly firing neurons, (II) the class of neurons where simple patterns are injected into a random or incompatible background, and (III) the class of neurons that preferentially fire in patterns. In Fig. 6(a), the three classes are illustrated by one V1 neuron each. Whereas bimodal ISI histograms emerge in all cases, the corresponding log-log plots indicate clear differences in the associated firing behaviors.

Whereas neurons of class I show straight-line correlation plots whose slope fails to saturate, neurons from class II show a dependence of the slope-ratio on the embedding dimension (cf. Fig. 2). The detailed analysis of the second neuron [see Fig. 6(b) and Table II] reveals ratio minima at $m=2$ and $m=3$, indicating that patterns of length 2 and 3 are present. The class III neuron's behavior is compatible (cf. Fig. 1) with the earlier finding [3] that members of this class are generally associated with two (exceptionally: one) clearly positive Lyapunov exponents, and with fractal dimensions that saturate as a function of the embedding dimension. These indicators hint at unstable periodic orbits generating these responses, and imply that the data are essentially deterministic in nature. Furthermore, representatives of class III have been found, where the optimal stimulus displayed pattern-sharpening effects [Fig. 6(c)].

The results obtained for the LGN data are compatible with the above classification, but the class properties are less well exhibited. An overview on the classification of investigated neuronal LGN and V1 data is shown in Fig. 7.

VI. DISCUSSION

Our method provides an unbiased test for pattern occurrence, even in noisy environments. It is simple to implement, and use. Although the method does not directly deliver the patterns, robust indicators for their lengths are provided. Together with the locations of the steps, this can be used to substantially minimize the set of templates to be tested. As multitrain patterns often imply single-train patterns, our findings are also of interest for analysis of the former.

Our experimental results show the abundance of patterns in neural spike trains, corroborating earlier reports [3,9,25–28]. Although this does not directly prove a functional role, spike patterns could serve as code words in neural information transfer [29]. In particular the deterministic nature of class III neuron responses (and to a lesser extent, that of class II) implies that patterns could be used as an efficient means of information transmission. The context of noise-driven computation by locking [30,31] provides a theoretical framework wherein both extreme classes I and III gain a straightforward functional justification. When LGN is compared to V1, an increased level of noise appears to be present. This property could indicate a simpler type of computation formed in the LGN. Correlation integral-based pattern detection provides an appropriate tool to further address this, and related, questions.

[1] C. Koch, *Biophysics of Computation* (Oxford University Press, Oxford, 1999).

[2] *The Handbook of Brain Theory and Neural Networks*, edited by M. A. Arbib (MIT Press, Cambridge, MA, 1998).

[3] R. Stoop, D. A. Blank, A. Kern, J.-J. van der Vyver, M. Christen, S. Lecchini, and C. Wagner, Cog. Brain Res. **13**, 293 (2002).

[4] P. Dayan, and L. F. Abbott, *Theoretical Neuroscience* (MIT Press, Cambridge, MA, 2001).

[5] R. Stoop, K. Schindler, and L. Bunimovich, Biol. Cybern. **83**, 481 (2000).

[6] F. Rieke, D. Warland, R. de Ruyter van Steveninck, and W. Bialek, *Spikes. Exploring the Neural Code* (MIT Press, Cambridge, MA, 1999).

[7] J. E. Dayhoff and G. L. Gerstein, J. Neurophysiol. **49**, 1334 (1983).

[8] I. V. Tetko and A. E. P. Villa, J. Neurosci. Methods **105**, 1 (2001).

[9] R. Lestienne and B. L. Strehler, Brain Res. **437**, 214 (1987).

[10] Y. Prut, E. Vaadia, H. Bergman, I. Haalman, H. Slovin, and M. Abeles, J. Neurophysiol. **79**, 2857 (1998).

[11] B. L. Strehler and R. Lestienne, Proc. Natl. Acad. Sci. U.S.A. **83**, 9812 (1986).

[12] P. Grassberger and I. Procaccia, Physica D **13**, 34 (1984).

[13] A. Kern, W.-H. Steeb, and R. Stoop, Z. Naturforsch., A: Phys. Sci. **54a**, 404 (1999).

[14] H. Kantz and T. Schreiber, *Nonlinear Time Series Analysis* (Cambridge University Press, Cambridge, England, 2000).

[15] F. Takens, in *Dynamical Systems and Turbulence*, Lecture Notes in Mathematics 898, edited by D. A. Rand and L. S. Young (Springer, Berlin, 1981), pp. 366–381.

[16] A. M. Fraser and H. L. Swinney, Phys. Rev. A **33**, 1134 (1986).

[17] J. Peinke, J. Parisi, O. E. Roessler, and R. Stoop, *Encounter with Chaos* (Springer, Berlin, 1992).

[18] M. Ding, C. Grebogi, E. Ott, T. Sauer, and J. A. Yorke, Physica D **69**, 404 (1993).

[19] T. Sauer, Phys. Rev. Lett. **72**, 3811 (1994).

[20] N. J. Corron, S. D. Pethel, and B. A. Hopper, Phys. Rev. Lett. **84**, 3835 (2000).

[21] R. Stoop and C. Wagner, Phys. Rev. Lett. **90**, 154101 (2003).

[22] N. Brenner, O. Agam, W. Bialek, and R. de Ruyter van Steveninck, Phys. Rev. E **66**, 031907 (2002).

[23] T. C. B. Freeman, S. Durand, D. C. Kiper, and M. Carandini, Neuron **35**, 759 (2002).

[24] R. Stoop, J.-J. van der Vyver, and A. Kern, in *Proceedings of the IEEE Conference on Nonlinear Dynamics of Electronic Systems NDES 2001*, 2001, pp. 113–116.

[25] J. E. Dayhoff and G. L. Gerstein, J. Neurophysiol. **49**, 1349 (1983).

[26] M. Abeles and G. L. Gerstein, J. Neurophysiol. **60**, 909 (1988).

[27] R. Lestienne and H. C. Tuckwell, Neuroscience **1**, 315 (1982).

[28] I. V. Tetko and A. E. P. Villa, J. Neurosci. Methods **105**, 15 (2001).

[29] B. L. Strehler, Perspect. Biol. Med. **12**, 584 (1969).

[30] R. Stoop, K. Schindler, and L. A. Bunimovich, Acta Biotheor. **48**, 149 (2000).

[31] R. Stoop, D. A. Blank, J.-J. van der Vyver, and A. Kern, in *Proceedings of the IEEE European Conference on Circuit Theory ECCTD*, Vol. I, 2001, pp. 221–224.